A review of Radar Detection Fundamentals

Pape Sanoussy Diao, Thierry Alves, Benoit Poussot, and Sylvain Azarian

***Abstract*—A review of the radar detection literature, which permits engineers to size radar systems considering various fundamental parameters is presented in this paper. The mono-static radar equation is reviewed in detail and its different terms are explained. Its essential parameters are highlighted with evaluation means allowing to choose their values. Thus, the theoretical Swerling models are recalled for modeling the radar cross section (RCS) of targets. The fluctuations of the RCS and their probability densities are presented according to the models. In addition, some practical examples are outlined to give ideas on when to use the Swerling models. Signal-to-noise ratio (SNR) is discussed in relation to the reliability performance of radar systems, i.e. detection and false alarm probabilities, but also through fixed threshold and constant false alarm rate (CFAR) detection techniques. Equations and radar operating curves (ROCs) to estimate the SNR required to satisfy a given system performance are presented for the different target models. Radar signal integration techniques such as coherent integration, non-coherent integration, binary integration and cumulative detection are also discussed in the context of multiple-observation detection to improve performance. The principle of operation of each of these integration techniques is explained and the equations and ROCs are presented for the different Swerling targets. The various system losses that contribute to the reduction of radar echo energy and signal processing losses that increase the required SNR are also exposed. These losses are included into the radar equation to complete the sizing and allow a more realistic estimate of the detection range.**

***Index Terms*—Radar detection, Radar range equation, Radar Cross Section (RCS), Signal-to-Noise Ratio (SNR), Detection probability, False alarm probability, Detection threshold, CFAR detection, Radar signal integration, Radar loss.**

I. Introduction

SINCE its invention during the World War II, the use of radar has continued to grow in both military and civilian applications. In the military field, radars have long been used for surveillance, detection and tracking, early warning, weapons control (missile guidance and interception), etc. Most military applications are also used in the civilian field. This is the case for tracking radars, anti-collision radars or ground penetrating radars for the detection of buried targets. Moreover, there are weather radars and car speed detection radars. Nowadays, in the civilian field, radars are more and more used for transport safety with body scanners, but also in the medical field for fall detection and vital signs monitoring (breathing and heart rate). These various applications can use different radar topologies in terms of waveform (pulse, continuous wave CW or frequency modulated continuous wave FMCW), architecture or processing. However, they are almost based on the same basic principles and broadly use the same fundamentals for the sizing of their respective systems.

The sizing of radar systems is done through the radar equation, similar to the Friis equation for communication systems. The radar equation includes complex parameters that need to be addressed in detail to understand the operation and design of radar systems.

One of these parameters is the Radar Cross Section (RCS). RCS is a critical parameter that must be determined with great care. Different theoretical methods can be used to determine the RCS of targets, with some approximations. They include ray methods (geometric optics, geometric diffraction theory, etc.), current-based methods (physical optics, physical theory of diffraction, etc.) and other methods such as asymptotic or incremental methods [1]. By simulation the RCS can be estimated with electromagnetic softwares. For example, HFSS based on the finite element method or FEKO based on the method of moments. Measurement methods based on pulse approach or frequency scanning [2] are also used to determine the RCS of objects.

In addition to RCS, sizing of a radar system involves estimating the signal-to-noise ratio (SNR) required to ensure the detection of a target with a given detection and false alarm probabilities. These probabilities set the reliability of radar systems. They depend on the statistical distribution of signals at the output of the receiver according to the type of target to be detected and the detection technique used. These probabilities were studied in detail by Marcum [3] for non-fluctuating targets and Swerling [4] for fluctuating targets. Very often radar systems use simple fixed threshold detection, but adaptive threshold detection can also be used to maintain a constant false alarm rate (CFAR).

Furthermore, the detection performance depends on the duration of observation of the received signal and the detection technique. They are evaluated using the probabilities of detection and false alarm. The assessment of these probabilities has been discussed by Barton [5], DiFranco and Rubin [6], for different target models and according to the technique used to maximize detection performance.

In addition, it is necessary to include a number of losses for a more complete sizing of radar systems. These losses are various and must be taken into account depending on the application and the radar system architecture.

In the literature, radar detection is discussed under different approaches. For example, Skolnik [7] and Blake [8] have each detailed a procedure for calculating the radar detection range. In [9], Barton has discussed radar detection procedures through the assessment of integration losses in particular. Richards [10] addressed radar detection through the performances in

M. Diao is with MORPHEE+, E21 Croix-Rouge française, 21 rue de la Vanne, 92120 Montrouge, France (e-mail:p.diao@morphee.eu.com).

M. Alves is with the ESYCOM lab of Univ Gustave Eiffel, CNRS UMR 9007, F-77454 Marne-la-Vallée, France (e-mail:thierry.alves@esiee.fr).

M. Poussot is with the ESYCOM lab of Univ Gustave Eiffel, CNRS UMR 9007, F-77454 Marne-la-Vallée, France (e-mail:benoit.poussot@u-pem.fr).

M. Azarian is with MORPHEE+, Le Village By CA, 67 rue des Godrans 21000 Dijon, France (e-mail:s.azarian@morphee.eu.com).

terms of probability from the decision statistics. However, it is difficult to find a simplified analysis of the fundamental parameters for radar detection that would allow a complete design of the systems. Thus, this paper proposes a review of the literature to detail the essential parameters for the systems design, including the detection process, and the assessment of its reliability performance through detection and false alarm probabilties, signal integration techniques, and system and signal processing losses.

II. Sizing of Radar Systems

The sizing of a radar system necessarily requires knowledge of the radar equation and control of its parameters. To establish this equation, we consider the detection scheme described in Figure 1 to have a better understanding of the approach and the steps of our analysis. In the following, we do not consider signal amplification for simplification. This only simplifies the topology of the receiver, without any loss of generality.

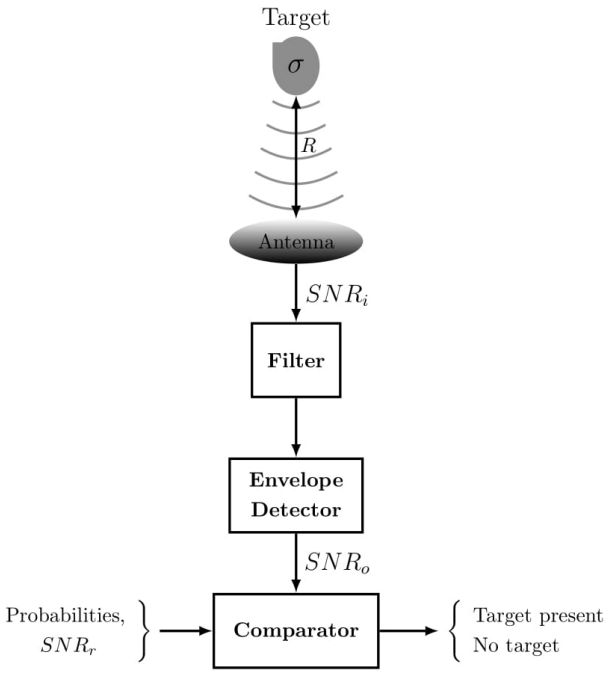

Fig. 1. Radar detection process chain (adapted from [9])

In an ideal detection process [9], the filter is matched to the waveform of the transmitted signal, whose parameters are known. However, if the signal waveform is not known, the filter can not be matched. In this case, the SNR is reduced compared to the first case due to the filter, but also the envelope detector [9]. In Figure, the signal at the filter input has a signal-to-noise ratio noted SNR_i. After the envelope detector, a time window is usually used to define the observation period based on the detectable target range. At the output of the detector, the SNR_i is degraded by the losses of the various receiver stages and is equal to SNR_o. The envelope of the detected signal is then compared to a threshold to decide whether a target is present or not. This detection threshold is chosen based on the probabilities defined in accordance with the desired performance in terms of system reliability.

The radar equation expresses the received power as a function of the characteristics of the transmitter, the receiver and the estimated RCS of the target, among others. Its basic form in a monostatic configuration is given by:

$$P_r = \frac{P_t G^2 \lambda^2 \sigma}{(4\pi)^3 R^4} \tag{1}$$

where P_t is the peak power of the radar transmitter, G the antenna gain, σ the RCS of the target and λ the operating wavelength. From this equation, the maximum range ($R_{\max}$) of the radar can be expressed for a received power equal to the receiver sensitivity also known as the minimum detectable power $S_{\min}$ [7]:

$$R_{\max}^4 = \frac{P_t G^2 \lambda^2 \sigma}{(4\pi)^3 S_{\min}} \tag{2}$$

Actually, equation (2) is very optimistic because it does not consider the different losses in the transmitting and receiving systems, but also complex environments. Furthermore, for a more realistic estimation of the range of radar systems, the statistical nature of the parameter $S_{\min}$ should be considered too. For this purpose, we will now study the influence of noise statistics on the sizing of radar systems.

In practice, $S_{\min}$ will be limited by the noise level. Indeed, the detection capability of a target depends not only on the power of the received signal, but also on the noise present in the receiver. Thus, a distinction is made between noise from the radar's external environment and the intrinsic noise of the receiver. In the absence of external noise sources, only thermal noise (or white noise) is considered. This noise is an unavoidable component generated by the thermal movement of conduction electrons in the resistive parts of the receiver input stages [7]. The thermal noise power at the antenna output N_{th} in Watt (W) is given by:

$$N_{th} = k_B T \Delta f \tag{3}$$

where $k_B = 1.38 \times 10^{-23}$ J/K is Boltzmann's constant, T is the temperature of the ohmic parts of the circuit in Kelvin (K) and Δf is the receiver bandwidth in Hz.

Since receivers are not ideal, they are characterized by their noise factor (F), which quantifies the degradation of the signal-to-noise ratio between their input and output:

$$F = \frac{SNR_i}{SNR_o} \tag{4}$$

where SNR_i and SNR_o are the signal-to-noise ratios at the input and output of the receiver, respectively.

The total noise power at the receiver output is given by the product of its noise factor and the input thermal noise power as shown by equation (5). For most receivers Δf represents the bandwidth of the intermediate frequency (IF) filter. T is usually taken at 290 K by radar operators.

$$N = k_B T \Delta f \cdot F \tag{5}$$

The minimum detectable power, which corresponds to that of the signal at the receiver input for a minimum SNR_o (see Figure 1) equal to the required SNR (SNR_r) is given by:

$$S_{\min} = k_B T \Delta f \cdot F \cdot SNR_r \tag{6}$$

The maximum range of the radar can then be written as a function of the SNR_r at the output of the receiver:

$$R_{\max}^4 = \frac{\boldsymbol{P_t} G^2 \lambda^2 \sigma}{(4\pi)^3 k_B T \boldsymbol{\Delta f} \cdot F \cdot SNR_r} \tag{7}$$

Equation (7) shows that the detection of a target with RCS σ at a given range R requires that the reflected signal has a signal-to-noise ratio SNR_o at the output of the detector at least equal to SNR_r (see Figure 1). In addition, equation (7) allows us to highlight the different parameters we have to adjust to optimize the performance of the radar. For example, in order to increase the range, a higher transmit power can be used, or the receiver sensitivity can be increased within a certain limit. Transmit power and antenna gain may be limited by frequency band standardization. The receiver bandwidth is defined by the filter. In practice, this bandwidth corresponds to the spectral occupancy of the transmitted signals, which defines the range resolution of the radar: $\delta R = c/(2\Delta f)$. In conventional radar, the bandwidth of transmitted signals is defined by their duration $\tau : \Delta f \approx 1/\tau$. As a result, the transmitted energy of the radar $P_t \cdot \tau$ is coupled to the range resolution δR. Thus, maximizing the range $R_{\max}$ results in increasing the duration of the transmitted signals, which degrades the range resolution δR. To overcome this problem, most modern radars use pulse compression to decouple the transmitted energy from the range resolution. Thus, the average power P_{av} is used in the radar equation rather than the peak power P_t:

$$R_{\max}^4 = \frac{\boldsymbol{P_{av} T_r} \cdot G^2 \lambda^2 \sigma}{(4\pi)^3 k_B T \cdot F \cdot SNR_r} \tag{8}$$

The average power is related to the peak power by $P_{av} \cdot T_r = P_t \cdot \tau$, with T_r the repetition period of the transmitted signals. Note that in pulse radars $\tau \ll T_r$, while in FMCW radars $\tau = T_r$. In equation (8), all parameters except the RCS can be more or less controlled by the radar designer. The choice of SNR_r is based on the desired performance in terms of system reliability. Thus, for a more complete sizing of radar systems, it is necessary to understand the phenomenology of target RCS.

III. Radar Cross Section

Depending on the behaviour of their RCS, one can consider two types of targets: fluctuating targets and non-fluctuating targets. Furthermore, targets are classified according to Swerling models.

A non-fluctuating target (also called Swerling 0, Sw-0 or Swerling V, Sw-V) has a RCS that is invariant in all directions. This is typically the case for the sphere. Since the RCS is constant, its probability density is given by a Dirac distribution centered at the RCS value.

A target is said to be fluctuating when its RCS is not constant. The RCS of a target often varies according to its orientation over time. Thus, it can fluctuate in amplitude (scintillation) and/ or in phase (glint). In this study, we will limit ourselves to amplitude fluctuation. Swerling has developed four fluctuating target models in [4]. The fluctuation of a target depends mainly on its size, shape and orientation over time. It is characterized by the speed of the fluctuation and its statistical distribution.

The RCS of a fluctuating Swerling I (Sw-I) target illuminated by a pulse beam is constant over the time of a scan, but changes from scan to scan. In other words, target echoes from the same scan are fully correlated, but independent between two scans.

A target probed by a group of pulses is said to be Swerling II (Sw-II) when its RCS varies from one pulse to another. In this case, the different echoes coming from the target are decorrelated. This type of target has a faster fluctuation than the Sw-I model.

For both fluctuation Sw-I and Sw-II models, the probability density of the target RCS is described by (9) [4], which corresponds to the chi-square law with 2 degrees of freedom.

$$w(\sigma, \overline{\sigma}) = \frac{1}{\overline{\sigma}} \exp\left(-\frac{\sigma}{\overline{\sigma}}\right) \tag{9}$$

where σ represents the RCS of the target and $\overline{\sigma}$ the average of σ over all fluctuations of the target.

Fluctuating targets are complex objects that sometimes have several scattering or bright spots. The Sw-I and Sw-II fluctuation models apply when these scattering points are independent and have approximately the same scattering surfaces. However, when a target has a larger scattering point than the others, the Swerling III (Sw-III) or Swerling IV (Sw-IV) model is used to characterize its fluctuation law. When such a target has a slow fluctuation (from one scan to another), it is referred to as a Sw-III target. The Sw-IV model is similar to the Swerling II case (fast fluctuation) but for targets with a predominant scatterer compared to the other scattering points.

The probability density of the RCS of a Sw-III target is identical to that of the Sw-IV model and is described by the chi-square law with 4 degrees of freedom [4], given by equation (10).

$$w(\sigma, \overline{\sigma}) = \frac{4\sigma}{\overline{\sigma}^2} \exp\left(-\frac{2\sigma}{\overline{\sigma}}\right) \tag{10}$$

Figure 2 illustrates the RCS fluctuation for Swerling targets and their probability density functions. Besides the differences in fluctuations, scan by scan (Sw-I & Sw-III) or pulse by pulse (Sw-II & Sw-IV), a high fluctuation of σ around its mean value $\overline{\sigma}$ (dashes lines) can be distinguished for Sw-I and Sw-II targets compared to the fluctuations of Sw-III & Sw-IV targets, due to the predominance of one of the scattering points.

Moreover, it should be noted that there are other models of fluctuating targets such as Weinstock's models described as specific cases of chi-square distribution and those described by Log-normal distribution [11]. In this paper, we have limited our study to the Swerling models, which beyond being the best known in radar, are relatively simple and allow us to understand the phenomenology of RCS fluctuation without loss of generality.

Swerling targets are theoretical models. In practice, it is difficult to determine the exact model of a target. Thus, the Sw-0 model is often associated with small targets that can be contained within a range bin (or range cell, which is defined by the range resolution δR) and whose RCS fluctuation is

This article has been accepted for publication in a future issue of this journal, but has not been fully edited. Content may change prior to final publication. Citation information: DOI 10.1109/MAES.2022.3177395, IEEE Aerospace and Electronic Systems Magazine

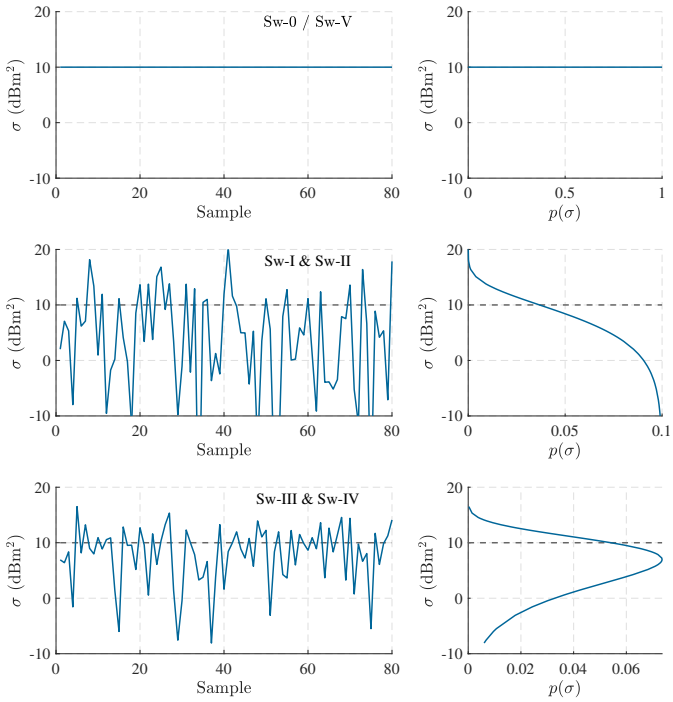

Fig. 2. RCS and probability density for different Swerling targets

very small. The Sw-I to Sw-IV models generally correspond to extended targets (spread over two or more range bins) and/or to targets moving more or less fast with respect to the repetition period of the signals transmitted by the radar. In addition, due to the frequency dependence of the RCS, some radar systems use frequency agility (altering the radar carrier frequency over shorter intervals) or frequency diversity (transmitting and receiving signals on two or more different frequency channels) to see the target as an Sw-II model. In this case, the choice of transmitted frequencies must consider certain parameters of the target (such as size, orientation with respect to the radar, etc.) in order to ensure decorrelation (independence) of its echoes at the different frequencies.

To take realistic examples, let's note that for detecting a tennis or bocce ball, the Sw-0 model is well adapted. On the other hand, for the detection of a moving rugby ball, the model can become complex. Indeed, with a double angular dependence of the RCS (ellipsoidal shape), we can expect a Sw-I or Sw-II fluctuation model according to the speed of the ball movement compared to the repetition period of the transmitted signals by the radar. A more complex case is the detection of a pedestrian by a radar having a range resolution lower than the body size (extended target). Considering the torso as the predominant scattering point compared to the others (legs, arms, head, etc.), the pedestrian is expected to behave as a Sw-III or Sw-IV target, again depending on the speed of its displacement compared to the repetition period of the signals transmitted by the radar.

Considering the complexity of RCS phenomenology due to a number of parameters (geometry, size or orientation of the objects, but also frequency and polarization of the radar antenna), simplifications are often used to estimate RCS of objects. For example, the object will be considered to have a single scattering point. In addition, the object is assumed to fit inside a single range bin, thus avoiding the occurrence of multiple scattering points or some form of backscatter spread. On the other hand, we will often stand in far field to assume the plane wave case for simplifications. Note that the approximations for estimating RCS will depend on the type of application and the level of complexity required. In this regard, it is easy to understand that estimating the RCS of a person in motion does not need the same requirements as estimating the RCS of a metal object in a bag left at a train station or airport.

IV. Radar Detection Process

In section II we saw that knowing the signal-to-noise ratio at the output of the receiver is required to estimate the radar detection range. In particular, a target is considered to be present when its echo has an SNR_o at least equal to the SNR_r or an equivalent amplitude greater than or equal to the detection threshold (η). The determination of the SNR_r or the detection threshold involves the assessment of the system reliability performance through the probability of detection (P_D) and the probability of false alarm (P_{FA}). These probabilities are determined through a statistical study of the radar echo signals.

A. Detection and Decision Theory

The main objective of a radar is to detect targets in a given environment. In most cases, parisitic echoes (clutter) and thermal noise are added to the reflected signal at the receiver. Because of the random nature of noise and clutter, radar detection is based on statistical decision theory [6]. The objective of this theory is to set a decision rule based on the hypotheses of absence H_0 and presence H_1 of the target. These hypotheses are defined according to the composition of the radar echo y:

$$\begin{aligned} H_0 &: y = n \\ H_1 &: y = s(\zeta) + n \end{aligned} \tag{11}$$

where n is additive noise and s is a useful signal reflected from a target. ζ represents the parameters of the useful signal (amplitude, phase, velocity, direction, etc.). Under H_0, the received signal is assumed to contain only noise with a probability density $p(y|H_0)$. Under H_1, it is assumed that the received signal contains a useful signal coming from a target, but immersed in noise. Its probability density is then written $p(y|H_1)$.

In reality, radar detection is based on a detector. The objective is then to maximize P_D while minimizing errors (among others P_{FA}). In practice, it is very difficult to get rid of errors, in particular when one does not know the statistics of the environment around the radar and the nature of the objects to be detected. To minimize these errors, decision criteria such as Bayes decision rule, Minimax approach or Neyman-Pearson criterion [6] [12] are used.

The Bayes decision rule is applied when the a priori probabilities of the assumptions are known. In contrast, the minimax approach can be used when the a priori probabilities

This article has been accepted for publication in a future issue of this journal, but has not been fully edited. Content may change prior to final publication. Citation information: DOI 10.1109/MAES.2022.3177395, IEEE Aerospace and Electronic Systems Magazine

of the assumptions are not known, however it is based on costs associated with decisions. In practice, and particularly in the radar context, the a priori probabilities of the assumptions are generally unknown and it is very difficult to assign realistic costs to the decisions made. In this case, the Neyman-Pearson criterion is more appropriate for the detection process, as it does not require a priori knowledge of signal statistics or cost attribution. This criterion is based on the likelihood ratio, noted $\Lambda(y)$ and defined by the ratio of the probability densities under the assumptions H_1 and H_0:

$$\Lambda(y) = \frac{p(y|H_1)}{p(y|H_0)} \underset{H_0}{\overset{H_1}{\gtrless}} \eta \tag{12}$$

Thus, a target is declared present when $\Lambda(y)$ exceeds the detection threshold η and absent otherwise. The choice of the threshold depends on the required probability of false alarm:

$$P_{FA} = \int_{\eta}^{\infty} p(y|H_0)dy \tag{13}$$

When the threshold is determined, the probability of detection is calculated by:

$$P_D = \int_{\eta}^{\infty} p(y|H_1)dy \tag{14}$$

The likelihood ratio test (LRT) described in (12) is based on simple assumptions where the probability densities of signals are known. However, in most practical cases, the probability density under each assumption depends on a set of unknown parameters (amplitude, phase, etc.). Therefore, under each hypothesis the signal y is described by a mixture of probability densities. In this case, the hypotheses are no longer simple, they are said to be multiple. Consequently, the likelihood ratio (12) cannot be applied. Thus, to get back to simple hypotheses we use the generalized likelihood ratio [13] given by:

$$\Lambda(y,\theta) = \frac{p(y|H_1,\hat{\theta}_1)}{p(y/|H_0,\hat{\theta}_0)} \underset{H_0}{\overset{H_1}{\gtrless}} \eta \tag{15}$$

where $\hat{\theta}_i = \arg\max_{\theta} p(y|H_i,\theta)$ represent the set of estimated parameters that maximizes the likelihood of the data under each hypothesis. Then, the detection procedure can be reduced to a Generalized Likelihood Ratio Test (GLRT). Details on the development of the LRT and the GLRT are beyond the scope of this paper. However, for greater depth on their uses from a practical point of view, the reader is invited to refer to the well known literature [6] and [10].

B. Fixed Threshold Detection

Fixed threshold detection is generally used in radar for simple configurations. It consists in comparing the radar echo (or target return) signal level at the output of the detector to a fixed threshold, as shown in Figure 3. The signal y consists in Z samples, each of which corresponds to a range bin. Thus, a target will be considered to be present in the range bin i, if y_i is greater than or equal to the detection threshold η and absent otherwise. The detection threshold depends on the noise power (calculated in equation (5), which we note here β^2), but also on the P_{FA}, whose estimation depends on the distribution of the signal y according to the fluctuation model of the target to be detected.

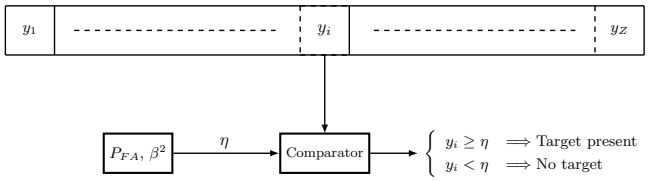

Fig. 3. General scheme of a fixed threshold detection

1) Probability densities: In this subsection we lead a statistical study of radar echoes to illustrate the principle of threshold detection using probability density functions. For this, we consider an independently and identically distributed complex white Gaussian noise whose components I and Q each have a zero mean and $\beta^2/2$ of variance. The total noise power is then β^2. The probability density of each of the components is written as:

$$p(x) = \frac{1}{\sqrt{\pi\beta^2}} \exp\left(-\frac{x^2}{\beta^2}\right) \tag{16}$$

where x represents the noise voltage.

By considering only noise at the receiver input of Figure 1 and assuming that the filter bandwidth Δf is small relative to its center frequency, the corresponding noise envelope at the output of the linear detector follows a Rayleigh probability density [3] [14]:

$$p_n(y) = \frac{2y}{\beta^2} \exp\left(-\frac{y^2}{\beta^2}\right) \tag{17}$$

where y is the amplitude of the noise envelope at the output of the detector. Note that in the case of a square law detector, the noise envelope follows an exponential density [5].

Now let's assume at the input of the filter a sinusoidal signal of duration $1/\Delta f$ corrupted by noise. The probability density of the output signal envelope from the linear detector is then given by [14]:

$$p_s(y) = \frac{2y}{\beta^2} \exp\left(-\frac{y^2+a^2}{\beta^2}\right) I_0\left(\frac{2ya}{\beta^2}\right) \tag{18}$$

where a is the amplitude of the signal in the absence of noise and I_0 is the modified Bessel function of first kind and zero order. Equation (18) is a Rice probability density. In the absence of signal, it is equal to the Rayleigh probability density given in (17).

Figure 4 illustrates the principle of threshold detection using probability density functions by considering the probabilities P_D and P_{FA} as defined in (13) and (14) respectively. To decrease the P_{FA}, the detection threshold η can be increased. However, this also results in a decrease of P_D. As in radar detection, the goal is to increase P_D while minimizing P_{FA}, a trade-off is therefore necessary in the choice of these probabilities.

This article has been accepted for publication in a future issue of this journal, but has not been fully edited. Content may change prior to final publication. Citation information: DOI 10.1109/MAES.2022.3177395, IEEE Aerospace and Electronic Systems Magazine

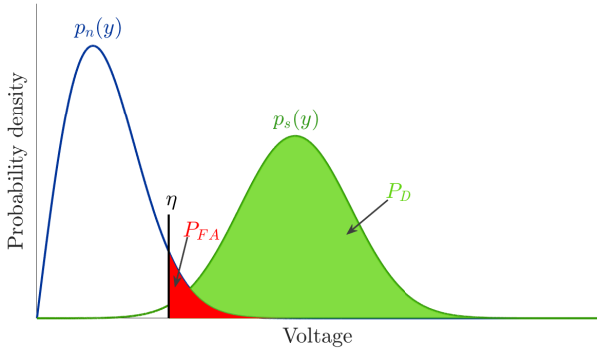

Fig. 4. Illustration of threshold detection by probability density functions

2) Probability, Threshold and SNR: In reality, radar detection is based on a detector. The operation of a detector depends on the threshold set according to the desired performance in terms of probabilities P_{FA} and P_D. In practice, a P_{FA} is set to compute the detection threshold η. From this threshold and the SNR, P_D is then evaluated. Equally, from η and the desired P_D, the SNR_r is determined.

Starting from (13) and replacing $p(y|H_0)$ by $p_n(y)$ defined in (17), one easily expresses the P_{FA} and then the voltage detection threshold η as shown in equations (19) and (20) respectively. For a targeted P_{FA} (for example 10^{-6}), the detection threshold is easily calculated if the noise power is known.

$$P_{FA} = \exp\left(-\frac{\eta^2}{\beta^2}\right) \tag{19}$$

$$\eta = \sqrt{-\beta^2 \ln\left(P_{FA}\right)} \tag{20}$$

The expression of P_D is obtained in several steps. By replacing in (14) $p(y|H_1)$ by $p_s(y)$ in (18), we obtain (21), then (22) by using the Marcum function Q_M [15]:

$$P_D = \int_{\eta}^{\infty} \frac{2y}{\beta^2} \exp\left(-\frac{y^2+a^2}{\beta^2}\right) I_0\left(\frac{2ya}{\beta^2}\right) dy \tag{21}$$

$$P_D = Q_1\left(\sqrt{\frac{2a^2}{\beta^2}}, \sqrt{\frac{2\eta^2}{\beta^2}}\right) \tag{22}$$

In (22), the term a^2/β^2 corresponds to the SNR. Thus, by replacing η by its expression established in (20), P_D can be simply written:

$$P_D = Q_1\left(\sqrt{2SNR}, \sqrt{-2\ln(P_{FA})}\right) \tag{23}$$

Equation (23) shows that P_D does not depend on the power of the noise, nor on that of the signal, but rather on the SNR. It thus allows us to evaluate the radar operating curves (ROCs) which express the P_D as a function of the SNR and the P_{FA}.

These curves are illustrated in Figure 5 for the classic case of the detection of a non-fluctuating target (Sw-0) based on a single radar echo. Each point of these curves corresponds to an SNR_r which makes it possible to size the radar systems from equation (8), according to the desired performance in terms of reliability (P_D and P_{FA}). For example, for $P_D = 90\%$ and

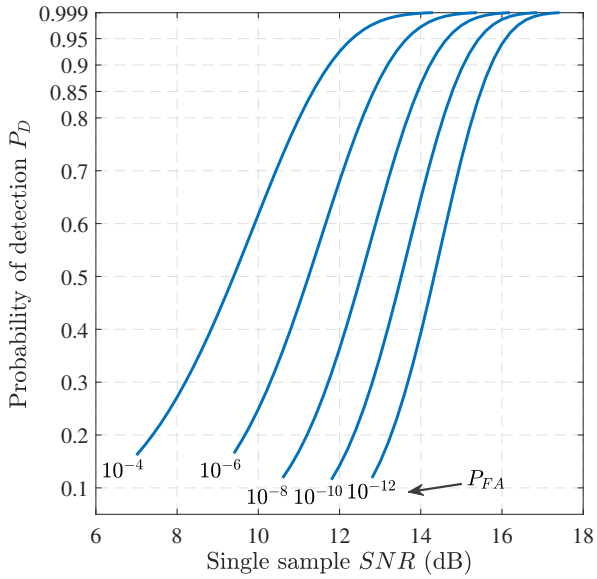

Fig. 5. ROC of Swerling 0 target for different values of P_{FA}

$P_{FA} = 10^{-6}$, the SNR_r is 13.2 dB. This value of SNR_r is a reference value in radar detection. Moreover, the choice of the P_{FA} can be determined as a function of the average accepted duration between two false alarms [7].

For fluctuating targets, detection probabilities were calculated by Swerling [4]. The expressions of these probabilities given in [4] [6] [10] are here rewritten to be expressed as a function of the P_{FA}. Due to the fluctuation laws described in (9) and (10), the detection probabilities are identical for targets Sw-I and Sw-II targets on the one hand, and Sw-III and Sw-IV on the other hand, because the detection is based on a single radar echo. The detection probability of a Sw-I or Sw-II target can be written as given by (24). When a fluctuating target is of type Sw-III or Sw-IV, its probability of detection can be expressed by (25). Note that for these expressions, SNR is the average signal-to-noise ratio over all fluctuations of the target.

$$P_D = \exp\left(\frac{\ln P_{FA}}{1+SNR}\right) \tag{24}$$

$$P_D = \left[1 - \frac{\ln P_{FA}}{(1+SNR/2)\,(1+2/SNR)}\right] \times \exp\left(\frac{\ln P_{FA}}{1+SNR/2}\right) \tag{25}$$

ROCs for fluctuating targets are given in Figure 6 in comparison with that of the non-fluctuating targets for $P_{FA} = 10^{-6}$. Unsurprisingly, it is clear that for $P_D > 40\%$, non-fluctuating targets are easier to detect. Indeed, for $P_D = 90\%$ and $P_{FA} = 10^{-6}$, the SNR_r for a Sw-I/II is about 8 dB higher than that of a Sw-0. For a Sw-III/IV target, the SNR_r is only 4 dB higher than that of a Sw-0 target. These differences in SNR_r relative to the Sw-0 correspond to the fluctuation losses of the targets.

The sizing of radar systems is generally done for a maximum detection range according to the RCS of the targets to be detected (see equation (8)). The detection threshold is

This article has been accepted for publication in a future issue of this journal, but has not been fully edited. Content may change prior to final publication. Citation information: DOI 10.1109/MAES.2022.3177395, IEEE Aerospace and Electronic Systems Magazine

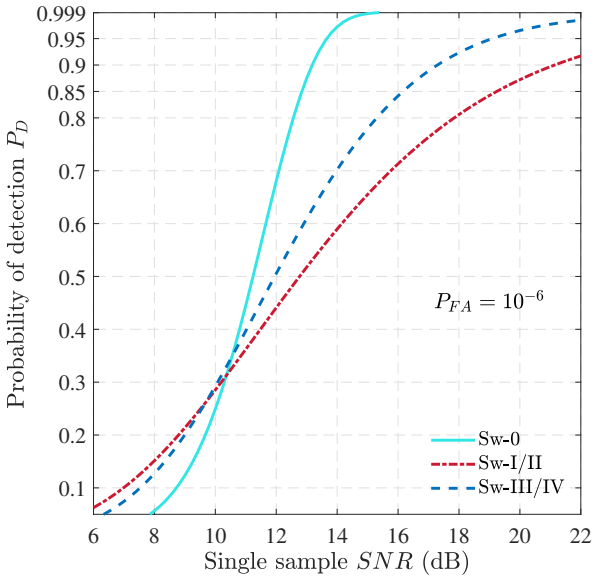

Fig. 6. ROC of Swerling targets with single sample detection

calculated for a required or acceptable P_{FA} from equation (20) for a linear envelope detector. P_D is then determined from the SNR of the target echo. Furthermore, equation (20) shows that the detection threshold is calculated from the power of the noise received by the radar receiver and corresponds to a fixed value. However, in practice the noise level may vary due to changes in the environment outside the radar, but also due to temperature drift of the receiver circuits [10] [16] and thus cause variations in the P_{FA}. When these variations are internal to the radar, they can be reduced by temperature compensation or by periodic calibration of the system. However, when the noise variations are mainly from external sources such as clutter interference or jamming, they can lead to severe variations in the P_{FA} and thus compromise the radar reliability. As an example, Richards [10] has shown that a 2 dB increase in noise power can lead to an increase in P_{FA} of 1.5 to 3 orders of magnitude, and the smaller the P_{FA} value, the greater the increase. The use of a fixed detection threshold is therefore not appropriate when the noise has variations from external sources. Therefore, adaptive threshold detection techniques are used to maintain a constant false alarm rate (CFAR).

C. Adaptive Threshold Detection: CFAR

CFAR processing [10] [17] [18] is used to find the correct detection threshold to compensate for spatial and temporal variations in noise, but also for the presence of clutter or interferences. They use a variable or adaptive detection threshold to maintain a constant false alarm rate. CFAR processing generally applies to y_i data at the output of the detector. Threshold determination is based in part on estimating the clutter plus noise level around the target. This is done using a sliding window (or reference window) with N_c cells, where each corresponds to a range bin. The data in the reference window is distributed around the cell under test, noted z as shown in Figure 7.

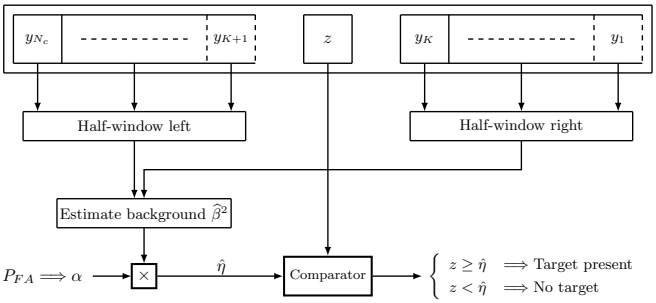

Fig. 7. General diagram of a CFAR detection procedure

The mean power of the estimated clutter plus noise $\widehat{\beta}^2$ is then calculated by considering only the data from the reference window. To estimate the detection threshold, $\widehat{\beta}^2$ is then multiplied by a weighting factor α calculated according to the P_{FA} required and the type of CFAR processing used. There are different types of CFAR processing, the best known of which are Cell−Averaging (CA) CFAR and Ordered Statistic (OS) CFAR. In the following, we will consider that the data are derived from a square law detection. White Gaussian Noise is also assumed, whose complex data are independently and identically distributed.

1) CA CFAR method: In the CA CFAR method, the estimation of clutter plus noise power is based on the arithmetic mean. However, since the energy of the echo from the same target may be distributed over several range bins and in this case may affect the clutter plus noise power estimation, a number of cells directly adjacent to the cell under test should not be considered. These cells are called guard cells, represented in a grid in Figure 8.

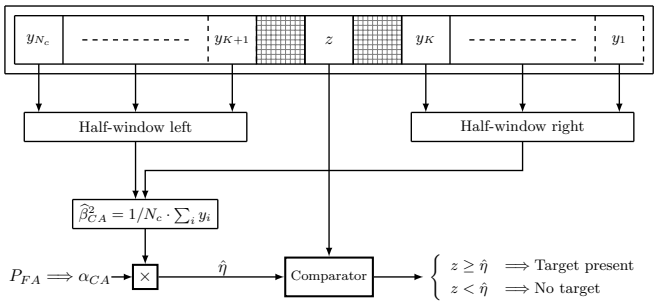

Fig. 8. Synoptic of a CA CFAR detection with two guard cells

The average clutter plus noise power is estimated by:

$$\widehat{\beta}^2_{CA} = \frac{1}{N_c} \sum_{i=1}^{N_c} y_i \tag{26}$$

where N_c is the total number of cells in the reference window. The calculation of the weighting factor for threshold determination is detailed in [10] [19]:

$$\alpha_{CA} = N_c \left(P_{FA}^{-1/Nc} - 1 \right) \tag{27}$$

The CA CFAR as presented here is based on the assumption of uniform clutter in the reference window. However, sometimes the clutter is not uniform in the reference window or only the edges of the clutter are contained in the

reference window. In this case, cell averaging CFAR with Greatest Of (GO) selection (CAGO CFAR) [20] [21] is more suitable than conventional CA CFAR. On the other hand, when another target is present in one of the cells in the reference window, the detection threshold with CA CFAR becomes so high that it is impossible to detect the target in the cell under test. In this case, cell averaging CFAR with Smallest Of (SO) selection (CASO CFAR) [21] [22] is recommended to correctly detect each of the two targets. These improved CA CFAR procedures allow for better detection especially when the reference window contains non-uniform clutter or transition zones from different sources of clutter, or signal from another target. However, when the clutter is very localized compared to the size of the reference window, the performances of these methods become contrasted because, in this case, the power of the clutter is underestimated, which can lead to its detection. Moreover, these methods are based on assumptions of a static reference window. Thus, for a more robust detection considering the different scenarios mentioned above and insensitive to changes in environmental statistics, Rohling [20] introduced the OS CFAR method.

2) OS CFAR method : In contrast to the CA CFAR method, which is based on all the reference window samples, the OS CFAR method uses a single sample for the estimation of clutter plus noise power. To do this, the samples in the reference window are first sorted in ascending order. Then, the k-th sample is selected to represent the average clutter plus noise power. In the OS CFAR approach, it seems irrelevant to consider guard cells, since in any case the reference window samples are sorted before the clutter plus noise power estimation. Figure 9 shows the synoptic of a OS CFAR detection.

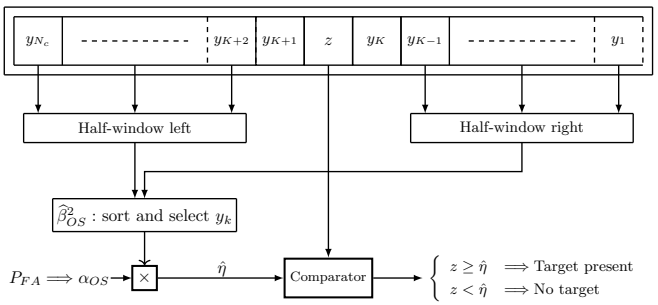

Fig. 9. Synoptic of a OS CFAR detection without guard cells

For the average clutter plus noise power estimation given in (28), Rohling [20] has shown that $k \approx 3N_c/4$ is suitable for practical applications.

$$\widehat{\beta}^2_{OS} = y_k, k \approx \frac{3N_c}{4} \tag{28}$$

The weighting factor α_{OS} is obtained by recursive calculation from the expression of the P_{FA} according to the value of k [10] [20]:

$$P_{FA} = k! C^k_{N_c} \frac{(\alpha_{OS} + N_c - k)!}{(\alpha_{OS} + N_c)!} \tag{29}$$

where $C^k_{N_c}$ is the binomial coefficient.

The OS CFAR method allows a correct detection of the targets independently of the clutter distribution or its location in relation to the reference window. It also allows the detection of several targets at the same time, while avoiding to detect clutter, even when it is localized enough in the reference window. Nevertheless, it should be mentioned that the use of a sorting algorithm makes the OS CFAR more complex to implement than other CFAR methods.

3) Performance of CFAR methods : The performance of detection methods is generally determined by the detection probabilities according to the type of target. However, CFAR methods are often evaluated in terms of losses. CFAR losses represent the increase of SNR_r (to guarantee a given P_D and P_{FA}) by a CFAR method compared to the case where the clutter plus noise power is assumed to be perfectly known (case of fixed threshold detection). This increase of the SNR_r allows to compensate the error on the estimation of the clutter plus noise level to guarantee the targeted P_D and P_{FA}. Indeed, without this increase of SNR_r, the P_D (resp. P_{FA}) would be relatively low compared to the case of fixed threshold detection for the same P_{FA} (resp. P_D). Since P_D depends on the type of target, CFAR losses should also depend on it. However, Nitzberg noted in [23] that CFAR losses are approximately the same when the target model is Sw-0, Sw-I or Sw-III. Since the detection is based on a single radar echo, Sw-II and Sw-IV targets will have the same losses. Therefore, the detection probabilities of a target model can be used to generalize the loss estimation.

The probability of detection of a Sw-I or Sw-II target by the CA CFAR method is given by [10] [24]:

$$P_D = \left(1 + \frac{\alpha_{CA}}{N_c\,(1 + SNR)}\right)^{-N_c} \tag{30}$$

In the case of a OS CFAR detection, the probability of detecting a Sw-I or Sw-II target [10] [25] is written:

$$P_D = k! C^k_{N_c} \frac{(\alpha_{OS}/\,(1 + SNR) + N_c - k)!}{(\alpha_{OS}/\,(1 + SNR) + N_c)!} \tag{31}$$

Figure 10 shows the ROCs of a Sw-I/II target obtained for a fixed threshold detection (Fixed Thd), CA CFAR and OS CFAR for $P_{FA} = 10^{-6}$. $N_c = 24$ and k is taken to be $3N_c/4$ for OS CFAR.

CFAR detection losses (L_d) are then evaluated as a function of N_c and relative to fixed threshold detection for $P_D = 90\%$ and $P_{FA} = 10^{-6}$ and presented in Figure 11.

CFAR losses decrease as the size of the reference window increases because the estimation of clutter plus noise levels becomes more accurate. Note that for given N_c and P_{FA}, CFAR losses increase with the probability of detection P_D. The losses shown in Figure 11 are higher with OS CFAR compared to CA CFAR because they correspond to a simple case with no target in the reference window. This situation is reversed in complex cases scenarii, for example, when interference targets are present in the reference window. For these cases, the authors suggest referring to [10] [26] [27] for more information.

The probabilities (P_D and P_{FA}) defined in this section are based on a single radar return and therefore correspond to a detection based on a single observation. To decrease the P_{FA} (i.e., minimize errors) the detection threshold can be increased.

This article has been accepted for publication in a future issue of this journal, but has not been fully edited. Content may change prior to final publication. Citation information: DOI 10.1109/MAES.2022.3177395, IEEE Aerospace and Electronic Systems Magazine

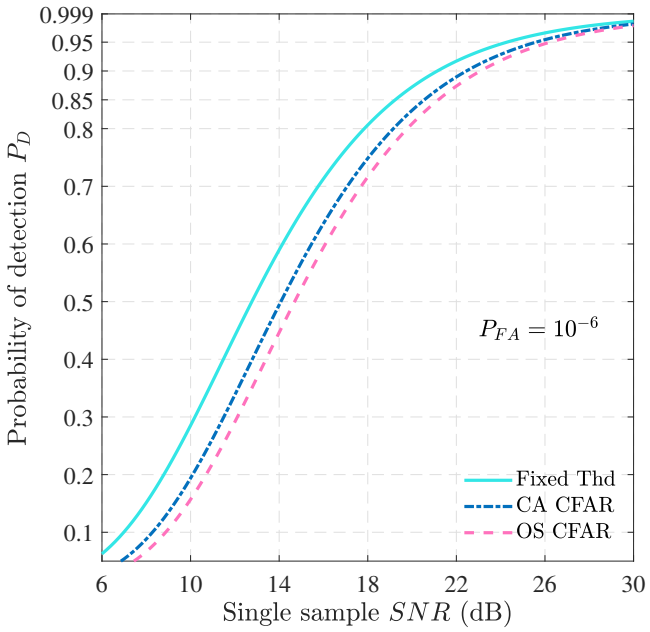

Fig. 10. ROC of Sw-I/II targets : comparison of detection methods

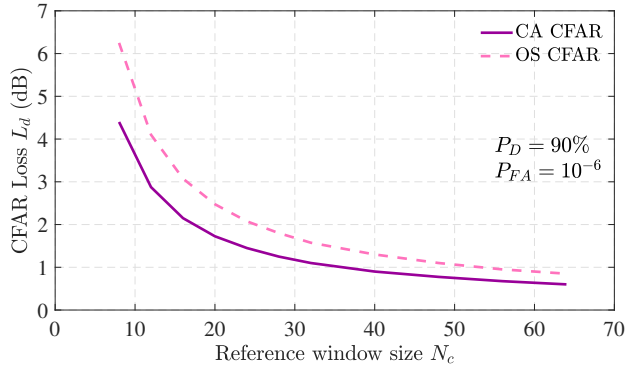

Fig. 11. CFAR loss relative to a fixed detection threshold as a function of the reference window size N_c

However, this results in an increase in the SNR_r, and thus a decrease in the maximum detection range, as it can be seen from equation (8). Thus, in order to improve system reliability (P_D and P_{FA}) without degrading the detection performance in terms of range, integration techniques are required.

V. Radar Signal Integration Techniques

Detection based on a single observation is not often used in radar, but it is taken as a reference, in particular to design radar systems under performance constraints in terms of probabilities and SNR_r. Integration techniques are generally used when the detection of a target is based on several echoes. In this case, it is called multiple-observation [6]. The process of integration consists of summing the radar echoes of a target in order to improve detection performance, particularly by reducing fluctuation losses when they are present. The transmitted radar waveform is identical over the duration of the observations. Echoes received during a number of observations for integration are assumed to come from the same target at the same bin. Integration process can be applied for each range, Doppler or angle (azimuth or elevation) bin.

Very often, coherent integration is confused with coherent processing and non-coherent integration with non-coherent processing. In fact, processing (coherent or non-coherent) is a process prior to integration. Coherent processing is generally used in radar because it allows Doppler processing, suppression of clutter and some parasitic echoes. On the other hand, when Doppler processing is not necessary, non-coherent processing can be used. In this paper, integration means combining (by summation) the signals after processing (coherent or non-coherent) to maximize the SNR before the detection process. Following coherent processing, coherent or non-coherent integration can be used. On a multiple-observation, the integration can be done on one or more processing intervals (PIs).

Starting from a multiple-observation detection, the probability density of the sum of N noise samples after square law detection is given by [3] [19]:

$$P_n(Y) = \frac{Y^{N-1}}{\Gamma(N)} \exp(-Y) \tag{32}$$

where $\Gamma(N) = (N-1)!$ is the Gamma function. Note that for $N = 1$, the noise envelope follows an exponential density as mentioned in Section IV-B1.

By using one of the standard forms of the Incomplete Gamma function γ_i, the probability of false alarm can be expressed as:

$$P_{FA} = 1 - \gamma_i(\eta_N, N) \tag{33}$$

where $\gamma_i(x, K) = [1/\Gamma(K)] \int_0^x u^{K-1} \exp(-u)\, du$ and η_N is the normalized detection threshold for a detection based on N noise samples. This threshold can be calculated recursively by solving equation (33) [28]. An approximation of the solution is given by (34) [19] [29]. Note that for $N = 1$, $\eta_1 \approx \ln(1/P_{FA})$, which corresponds to a normalized form of equation (20) when square law detection is used instead of linear detection.

$$\begin{aligned}\eta_N =& N - \sqrt{N} + 2.3\sqrt{-\log_{10} P_{FA}} \\ &\times \left(\sqrt{-\log_{10} P_{FA}} + \sqrt{N} - 1\right)\end{aligned} \tag{34}$$

After determining P_{FA} and η_N using equations (33) and (34) respectively, we can estimate the P_D according to the integration technique.

A. Coherent Integration

Coherent integration is based on summation in the complex domain, i.e. it preserves amplitude and phase of signals. In conventional receivers this type of integration is used before the envelope detector, it is called pre-detection integration. This integration requires phase coherence of the signals. That is to say a correlation of the different signals received during the integration time [16]. As a result, coherent integration seems more appropriate for Sw-0, Sw-I and Sw-III targets. Figure 12 presents the operating principle of coherent integration.

This article has been accepted for publication in a future issue of this journal, but has not been fully edited. Content may change prior to final publication. Citation information: DOI 10.1109/MAES.2022.3177395, IEEE Aerospace and Electronic Systems Magazine

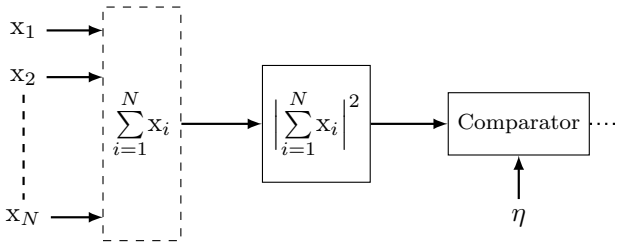

Fig. 12. Synoptic of a coherent integration

By coherently integrating a sequence of N samples (echoes, pulses), the signal-to-noise ratio is improved by a factor N.

$$SNR_N = N \cdot SNR \tag{35}$$

where SNR_N is the average signal-to-noise ratio per sample when N samples are coherently integrated and SNR is the signal-to-noise ratio per sample without any integration. Details of the calculation are provided in Appendix A.

Detection performance is then obtained from the detection probability equations for a single echo (Section IV-B2) with SNR equal to SNR_N. Coherent integration allows the SNR_r to be lowered by a factor N (corresponding to the integration gain, see Section V-F) for the same probabilities P_D et P_{FA} compared to conventional detection based on a single echo.

B. Non-coherent Integration

Non-coherent integration is based on the summation of the signal envelopes from a non-coherent detector. It is also called post-detection integration or video integration, as it is used after the envelope detector. Non-coherent detection can be quadratic (square law), linear or logarithmic [30]. Figure 13 presents the principle of operation of a non-coherent integration in the case of square law detection.

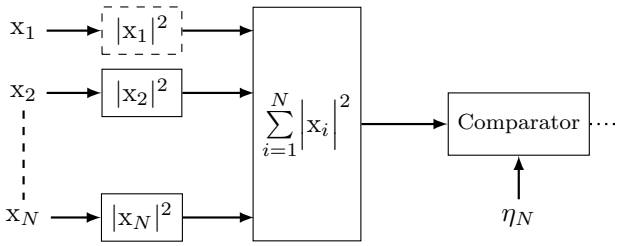

Fig. 13. Synoptic of a non-coherent integration

In practice, non-coherent integration will be more suitable for Sw-II and Sw-IV targets (for which the echoes are independent) as it does not require signal coherence because it destroys phase information.

The probability of detection after a non-coherent integration of N independent echoes resulting from square law detection was demonstrated by Marcum [3] for non-fluctuating targets (Sw-0), to be:

$$P_D = Q_N\left(\sqrt{NSNR}, \sqrt{2\eta_N}\right) \tag{36}$$

For fluctuating targets, Swerling has detailed the calculation of detection probabilities in [4]. In this article, the results are here rewritten to be expressed using the Incomplete Gamma function γ_i. Thus, for a Sw-I target, P_D after non-coherent integration of N echoes is expressed as:

$$P_D = 1 - \gamma_i\left[\eta_N, N-1\right] + \left(1+\frac{1}{NSNR}\right)^{N-1} \times \gamma_i\left[\frac{\eta_N}{1+1/NSNR}, N-1\right]\exp\left(\frac{-\eta_N}{1+NSNR}\right) \tag{37}$$

The expression of P_D obtained by non-coherent integration of N echoes from a Sw-II target is given by:

$$P_D = 1 - \gamma_i\left[\frac{\eta_N}{1+SNR}, N\right] \tag{38}$$

For a Sw-III target, P_D after non-coherent integration of N echoes is given in (39). This expression is approximative for $N > 2$, but as mentioned in [4] [6], it is sufficiently accurate for radar applications.

$$P_D \approx \left(1+\frac{2}{NSNR}\right)^{N-2}\left[1+\frac{\eta_N}{1+NSNR/2} - \frac{2}{NSNR}(N-2)\right]\exp\left(\frac{-\eta_N}{1+NSNR/2}\right) \tag{39}$$

One of the simplest forms of P_D expression obtained by non-coherent integration of N echoes from a Sw-IV target is given by DiFranco and Rubin [6]. It can be in the form:

$$P_D \approx 1 - \left(1+\frac{SNR}{2}\right)^{-N}\sum_{k=0}^{N}\left(\frac{SNR}{2}\right)^k C_N^k \times \gamma_i\left(\frac{\eta_N}{1+SNR/2}, N+k\right) \tag{40}$$

where C_N^k is the binomial coefficient. Note that unlike the formulation in [6], which uses the maximum SNR, in this article we use the average SNR as in [4].

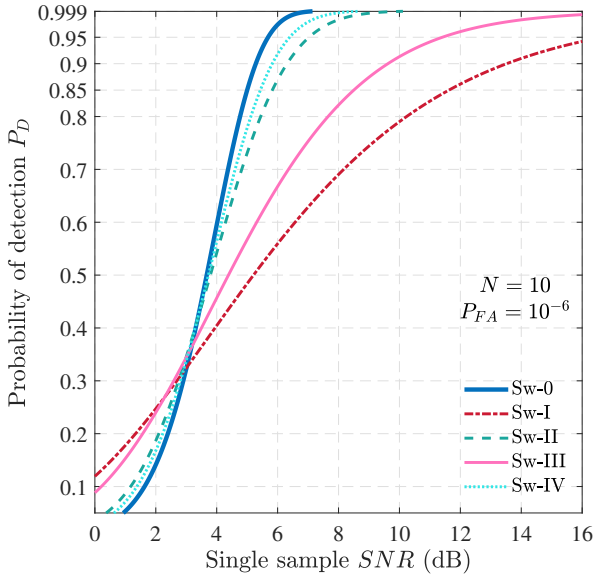

Fig. 14. ROC of Swerling targets with non-coherent integration ($N = 10$)

Figure 14 shows a comparison of detection probabilities obtained by non-coherent integration of $N = 10$ echoes for different targets with $P_{FA} = 10^{-6}$. Compared to detection

This article has been accepted for publication in a future issue of this journal, but has not been fully edited. Content may change prior to final publication. Citation information: DOI 10.1109/MAES.2022.3177395, IEEE Aerospace and Electronic Systems Magazine

based on single observation ($N = 1$), the non-coherent integration ($N = 10$) allows to reduce the SNR_r per sample by 7.6 dB for the Sw-I and Sw-III targets, about 8 dB for a Sw-0 target, 11.4 dB and 14.8 dB for the Sw-IV and Sw-II target respectively, and this for $P_{FA} = 10^{-6}$ and $P_D = 90\%$. As expected, non-coherent integration is more benefit for Sw-II and Sw-IV targets.

C. Binary Integration

Unlike non-coherent integration where the signal envelopes at the output of the detector are summed, in binary integration, the number of signals whose envelope exceeds a first detection threshold is counted [5] [6]. A target is then declared present when this number is at least equal to a second detection threshold. The detection is made on each of the N signals received by comparison with the first threshold η. The output of this comparator is then a sequence of N bits (0 or 1), hence the name binary integration. The decision is made by comparing the sum of the N bits with the second threshold M. Binary integration is a double threshold detection technique, also known as M-of-N detection. Figure 15 shows the operating scheme.

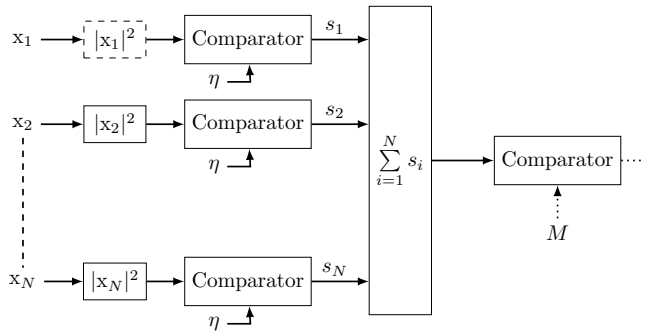

Fig. 15. Synoptic of a binary integration

For static and non-fluctuating targets, binary detection seems irrelevant because the target echoes are highly correlated. In this case, when the target is detected for one echo, it should be detected for all other echoes. However, it may be of interest, for example, to increase the reliability of detection by redundancy. For fluctuating targets this technique looks promising.

The probability that K samples exceed a fixed detection threshold among N independent samples of the same probability density is given by the binomial law (with probability of success P) [5] [6]:

$$P(K) = C_N^K P^K (1-P)^{N-K} \tag{41}$$

The overall probability of detection P_D in binary integration corresponds to the probability that K, the number of samples exceeding η, is greater than or equal to M $(1 \leq M \leq N)$. It is given by [6]:

$$P_D = \sum_{K=M}^{N} C_N^K P_d^K (1-P_d)^{N-K} \tag{42}$$

where P_d is the probability that each sample exceeds the threshold η. It is calculated from equation (23).

The overall probability of false alarm P_{FA} is obtained using (42) by replacing P_d by P_{fa}, the probability of false alarm per sample in relation to the threshold η. But, as $P_{fa} \ll 1$, it can be written [5] [10]:

$$P_{FA} \approx C_N^M P_{fa}^M \tag{43}$$

Equations (42) and (43) consider only non-fluctuating targets since the probability of detection P_d is assumed to be the same for each of the N signals. They are still valid for Sw-II [31] and Sw-IV [32] targets using equations (24) and (25) with P_d and P_{fa} instead of P_D et P_{FA} respectively. For Sw-I targets, Weiner described in [31] a simple procedure for assessing performance, based in particular on the fact that losses due to fluctuations are essentially independent on the integration gain. For Sw-III targets, the expression of P_D is given by Shnidman [32], but it is complex and requires numerical integration. However, considering the similarity of the fluctuations with the Sw-I targets (scan to scan fluctuation), Weiner's approach [31] can be used to evaluate the performance for the Sw-III targets without resorting to the exact numerical integration solution.

Performance of a binary integration depends on the two detection thresholds (η and M). In practice, the choice of these thresholds is made in order to maximize P_D for a given P_{FA} value. The calculation of the optimal value of M is given in [10] [32] for the different target models by $M_{opt} = 10^m N^v$, where m and v are given in Table I when $P_D = 90\%$ and $10^{-8} < P_{FA} < 10^{-4}$.

Figure 16 shows the detection curves obtained by binary integration with $N = 10$ and $M = M_{opt}$ for the different target models. For the Sw-I and Sw-III targets, the results are obtained using Weiner's approach [31]. Compared to detection based on a single observation ($N = 1$), binary integration ($N = 10$) allows to reduce the SNR_r by about 7 dB for Sw-0, Sw-I and Sw-III targets, about 10 dB for Sw-IV targets and about 13 dB for Sw-II targets, for $P_D = 90\%$ and $P_{FA} =$

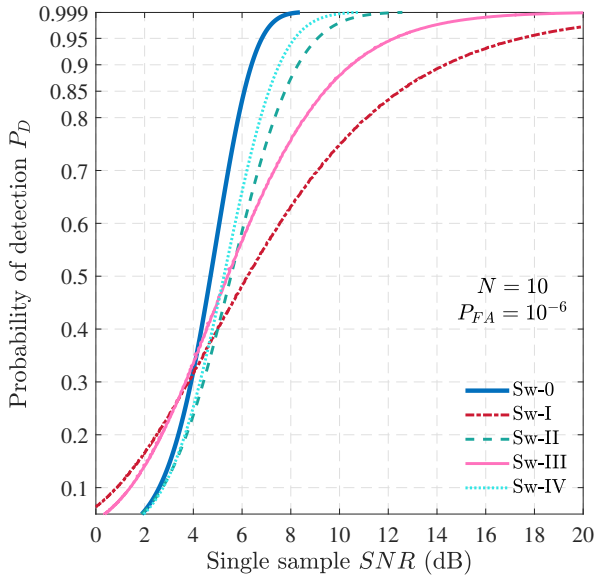

Fig. 16. ROC of Swerling targets with binary integration ($N = 10$, $M = M_{opt}$)

This article has been accepted for publication in a future issue of this journal, but has not been fully edited. Content may change prior to final publication. Citation information: DOI 10.1109/MAES.2022.3177395, IEEE Aerospace and Electronic Systems Magazine

TABLE I. PARAMETERS FOR ESTIMATING M_{opt} (FROM [10])

Target	m	v	N
Sw-0	0.8	-0.02	5-700
Sw-I	0.8	-0.02	6-500
Sw-II	0.91	-0.38	9-700
Sw-III	0.8	-0.02	6-700
Sw-IV	0.873	-0.27	10-700

10^{-6}. These results show that the performance improvement in binary integration is greater for fast fluctuating targets (Sw-II and Sw-IV), as well as for non-coherent integration. Binary integration is easy to implement compared to coherent or non-coherent integration, but it is less efficient.

D. Cumulative Detection

Cumulative detection is a special case of binary integration with $M = 1$. Thus, a target is declared present when at least one of the N samples exceeds the detection threshold η. As with binary integration, cumulative detection would be more efficient for fluctuating targets than for non-fluctuating targets due to the high correlation of echoes in the latter case. On the other hand, it seems to be more exposed to false alarms, since a single detection is sufficient to validate the decision.

The overall false alarm probability P_{FA} of a cumulative detection over a group of N samples, each having the same P_{fa}, can be deduced directly from equation (43) for $M = 1$:

$$P_{FA} \approx N P_{fa} \tag{44}$$

For Sw-0, Sw-II and Sw-IV targets, the cumulative detection probability P_D resulting from the detection of N independent samples of the same P_d, is written as [16] [32] [33]:

$$P_D = 1 - (1 - P_d)^N \tag{45}$$

where P_d is calculated from equations (23), (24) and (25) respectively for Sw-0, Sw-II and Sw-IV targets.

For Sw-I and Sw-III targets, expressions of cumulative detection probabilities can be deduced from the relationships given by Shnidman [32]. Thus, the expression given by Johnson [33] is obtained:

$$P_D = \int_0^\infty \left[1 - (1 - P_d)^N\right] w\left(x, SNR\right) dx \tag{46}$$

where $P_d = Q_1\left(\sqrt{2x}, \sqrt{-2\ln\left(P_{fa}\right)}\right)$ and $w\left(x, SNR\right)$ take the form of equations (9) and (10) for the Sw-I and Sw-III targets respectively, with SNR being the average signal-to-noise ratio over the N fluctuations of the target. The exact solution of equation (46) requires numerical integration. However, Weiner's approach [31] can be used to simplify the calculations with sufficiently accurate results for $P_D > 30\%$ (see Appendix B).

Figure 17 shows the cumulative detection probabilities obtained with $N = 10$ for the different target models.

These ROCs show that for $P_{FA} = 10^{-6}$ and $P_D = 90\%$, cumulative detection of $N = 10$ allows to reduce the SNR_r compared to an detection based on a single observation ($N = 1$) by about 3 dB for targets Sw-0, Sw-I and Sw-III, ≈ 7.5 dB for Sw-IV target and ≈ 11.5 dB for Sw-II target. On the other hand, the plots show that Sw-II and Sw-IV targets are easier to detect than Sw-0 targets in the case of cumulative detection for $N = 10$. These different results confirm that the performance improvement in cumulative detection is greater for rapidly fluctuating targets (Sw-II and Sw-IV), as well as for non-coherent integration and binary integration. Nevertheless, it should be noted that cumulative detection is globally less efficient than these other techniques.

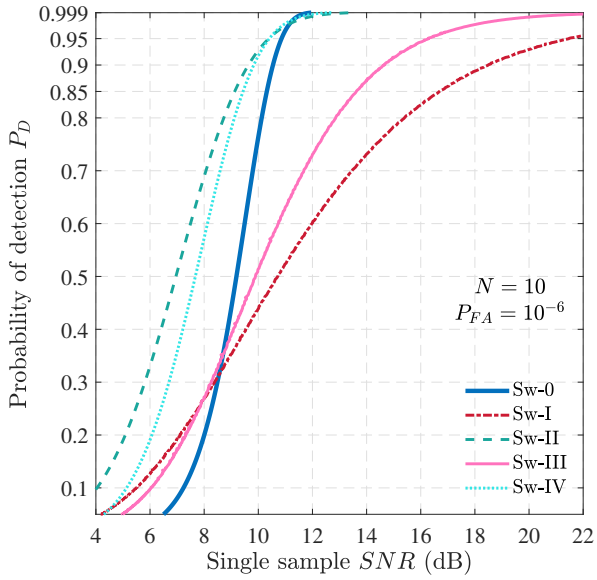

Fig. 17. ROC of Swerling targets with cumulative detection ($N = 10$)

E. The helpful Albersheim and Shnidman equations

The expressions established in the previous sections to estimate the required SNR for a given P_{FA} and P_D are complex. They can be easily implemented in suitable software for complete radar system sizing. For a quick assessment of the radar system performance, Albersheim and Shnidman have proposed a simplified approach avoiding the complex implementation [10].

1) Albersheim equation: The Albersheim equation is an empirical approximation to estimate for a non-fluctuating target the single sample required SNR according to P_{FA} and P_D, when integrating N independent samples in a non-coherent way, like equation (36). Unlike equation (36) which is determined with a square law detector, the Albersheim equation (47) is valid for a linear detector.

$$SNR\,[dB] = -5\log_{10} N + \left[6.2 + \left(\frac{4.54}{\sqrt{N + 0.44}}\right)\right] \times \log_{10}\left(A + 0.12AB + 1.7B\right) \tag{47}$$

where $A = \ln\left(0.62/P_{FA}\right)$ and $B = \ln\left(P_D/\left(1 - P_D\right)\right)$. For $P_{FA} \in [10^{-7}, 10^{-3}]$ and $P_D \in [0.1, 0.9]$, the error on the estimated SNR is less than 0.2 dB when $N \in [1, 8096]$.

2) Shnidman equation: The Albersheim equation is only valid for non-fluctuating targets (Sw-0 / Sw-V). This is an important limitation, because as can be seen in Figure 14, the

This article has been accepted for publication in a future issue of this journal, but has not been fully edited. Content may change prior to final publication. Citation information: DOI 10.1109/MAES.2022.3177395, IEEE Aerospace and Electronic Systems Magazine

SNR required for a non-fluctuating target is too optimistic when dealing with a fluctuating target, in particular Sw-I to Sw-IV. Thus, for all of the Swerling models, empirical approximations have been developed. These are summarized by the Shnidman equation (48) to determine the single sample required SNR, according to the P_{FA} and P_D probabilities. It is valid for a square law detector in the case of a non-coherent integration of N samples.

$$SNR = \frac{C \cdot X_\infty}{N} \tag{48}$$

where:

$$C\,[dB] = \begin{cases} C_1 & 0.1 \le P_D \le 0.872 \\ C_1 + C_2 & 0.872 \le P_D \le 0.99 \end{cases},$$

$$C_1 = \frac{P_D}{K}\left[\left(17.7006 P_D - 18.4496\right) P_D + 14.5339\right] - \frac{3.525}{K},$$

$$C_2 = \frac{1}{K}\left\{\exp\left(27.31 P_D - 25.14\right) + \left(P_D - 0.8\right) \times \left[0.7 \ln\left(10^{-5}/P_{FA}\right) + \left(2N - 20\right)/80\right]\right\},$$

$$K = \begin{cases} \infty & \text{Sw-0} \\ 1 & \text{Sw-I} \\ N & \text{Sw-II} \\ 2 & \text{Sw-III} \\ 2N & \text{Sw-IV} \end{cases},$$

$$X_\infty = \rho\left(\rho + 2\sqrt{\frac{N}{2} + \left(\kappa - \frac{1}{4}\right)}\right), \kappa = \begin{cases} 0 & N < 40 \\ 1/4 & N \ge 40 \end{cases},$$

$$\rho = \sqrt{-0.8 \ln\left(4 P_{FA}\left(1 - P_{FA}\right)\right)} + sign\left(P_D - 0.5\right) \times \sqrt{-0.8 \ln\left(4 P_D\left(1 - P_D\right)\right)}.$$

The function $sign(x)$ is 1 if $x > 0$ and -1 if $x < 0$. Note that in the case of a non-fluctuating target, $C = 1$. Regarding the error on the estimated SNR , a very nice comparison of the results of Albersheim's and Shnidman's equations is established by Richards in [10].

F. Comparison and Analysis

The different integration techniques described in this Section have advantages and drawbacks both in terms of implementation and efficiency. For desired performance P_D and P_{FA}, improvement of the SNR_r compared to detection based on a single observation depends on the target model. Thus, the choice of the integration technique will have to consider the system requirements in terms of implementation and complexity, but also the target fluctuation model in relation to the repetition period of the signals transmitted by the radar.

Regarding efficiency, the comparison of integration techniques can be made in terms of gain G_i or loss L_i [5]:

$$G_i\left(N\right) = \frac{SNR_r}{SNR_{rN}} = \frac{N}{L_i\left(N\right)} \tag{49}$$

where SNR_r et SNR_{rN} are the required SNR per sample respectively without integration and with integration of N samples, calculated for the same P_D and P_{FA}.

To quantify the effective contribution of the different integration techniques, we use the gain G_i. The same analysis can be done from losses L_i as presented in Appendix C for the case of Sw-0 targets. It is important to note that the contribution of integration is essentially the same for non-fluctuating targets (Sw-0) and slowly fluctuating targets (Sw-I and Sw-III) [5]. Indeed, Weiner's approach used in Sections V-C and V-D is based in part on this observation. As a result, the integration gains presented in Figure 18 are also valid for Sw-I and Sw-III targets. For Sw-II and Sw-IV targets, the integration gains are compared in Figures 19 and 20 respectively.

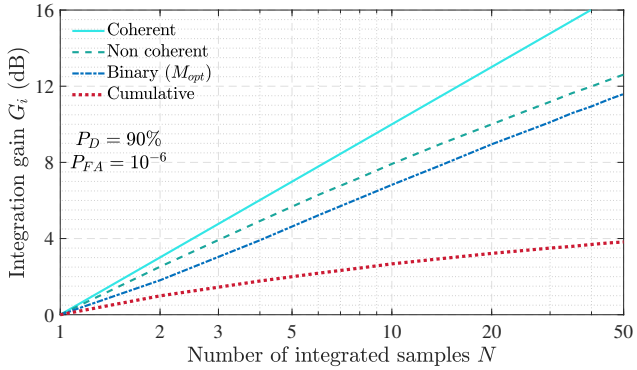

Fig. 18. Comparison of integration gain for Sw-0 targets

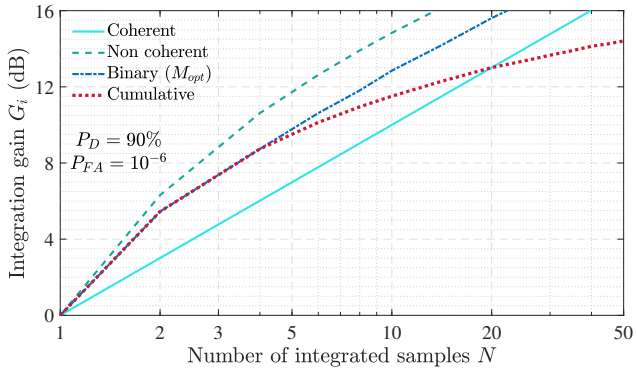

Fig. 19. Comparison of integration gain for Sw-II targets

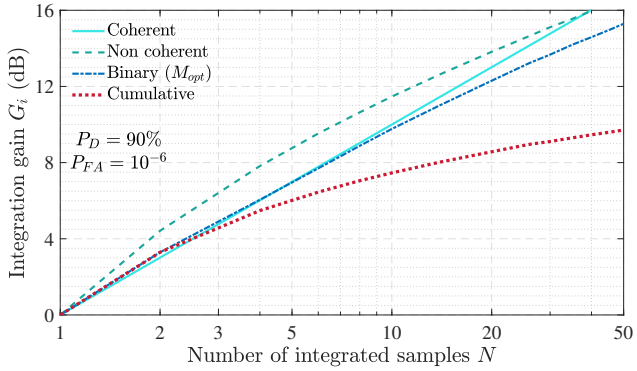

Fig. 20. Comparison of integration gain for Sw-IV targets

For Sw-0, Sw-I and Sw-III targets (see Figure 18), coherent integration is more efficient, followed by non-coherent integration, binary integration and cumulative detection, respectively.

In fact, with non-coherent integration, the effective improvement of the SNR compared to detection based on single observation is equal to N (the number of samples integrated) as with coherent integration. However, losses of the envelope detector used prior to the non-coherent integration process (see Figure 13) reduce the SNR, resulting in a lower gain [5]. Note that these losses are not inherent to non-coherent integration; they are simply related to the location of the envelope detector before the integration itself. These losses also partly explain the lower gains for binary integration and cumulative detection. In these two cases, another part of the losses would come from the compensation of the P_{FA}, which becomes relatively small due to the fact that the detection is only based on a certain number of samples ($< N$). They are more important with cumulative detection since this case is based on a single sample. For Sw-II targets (see Figure 19) the non-coherent integration offers a better gain for $P_D = 90\%$ and $P_{FA} = 10^{-6}$. We note that for $N \leq 4$, binary integration and cumulative detection have the same contribution, while coherent integration is less efficient for $N < 20$. Cumulative detection becomes less efficient than binary integration for $N > 4$ and coherent integration for $N > 20$.

For Sw-IV targets (see Figure 20), non-coherent integration is also more efficient up to $N \approx 40$, coherent integration being better for $N > 40$. For $N < 10$, binary integration has the same gain as coherent integration, which becomes more efficient for $N > 10$.

Coherent integration is preferred over each PI for the Sw-0, Sw-I and Sw-III targets. Since the echoes are correlated, the SNR in the target range bin can be maximized by coherent summation. On the other hand, when Sw-II or Sw-IV targets are present, non-coherent integration will be preferred on each PI, because it will allow a much greater improvement of the SNR in the target range bin compared to coherent integration. In fact, since the echoes are independent, the idea is simply to maximize the energy in the target range bin. As for non-coherent integration, binary integration is more efficient for Sw-II and Sw-IV targets in terms of SNR improvement, but its performance is less than the non-coherent integration, even when the choice of the second detection threshold is optimized. In addition, it does not require to keep track of all the signals, as only the result of thresholding (0 or 1) is required for the detection. Cumulative detection seems even simpler in its implementation, as it is based on a single detection for all the echoes considered. It offers better performances for Sw-II and Sw-IV targets. However, it is less efficient than binary integration.

As guidelines for real application, let us outline some examples. For resolved targets whose echoes are strongly correlated during the PI, coherent integration will be suggested. Indeed, when the target is resolved, its contributions will be located in the same range bin during the PI. Thus, due to the correlation of echoes, coherent integration (with a better gain) will allow a better improvement of the SNR in the target's range bin. For extended targets whose echoes are independent, non-coherent integration will be suggested. In fact, when a target is extended, its energy is spread over several range bins. Thus, the non-coherent integration of the target's echoes maximizes the SNR, especially in the range bin where the contributions of the target's scattering points are the highest. This would not be evident with coherent integration, because some kind of destructive interference could occur in the range bin of the predominant scattering points to the benefit of the other range bins, thus biasing the detection range. Note that binary integration and cumulative detection is often used by necessity, in particular contexts. For example, let us consider an observation time of several PIs with Sw-I or Sw-III targets. By using after Doppler processing a coherent integration in each PI (due to the correlation of the echoes), we obtain a single signal for each of the PIs. Thus, for detection, we can use a non-coherent integration of all the signals resulting from the different PIs, since the echoes are independent from one PI to another (here it is assumed that the duration of the processing interval is equivalent to that of a scan). However, to simplify processing, we can use binary integration, rather than non-coherent integration. The same approach can be used with Sw-II or Sw-IV targets, with the difference that instead of using coherent integration in each PI, non-coherent integration would be preferred, because in this case the echoes are independent in the same PI.

In summary, if the choice of the integration technique is fundamentally based on the RCS fluctuation model (echoes are correlated or not), it is no less important to take into account the spatial spread of the target (resolved or not), or the constraints required in terms of simplicity of implementation or the architecture of the radar system.

VI. Other Important Parameters

For a more rigorous analysis of radar detection, particularly in terms of range, other important parameters should be considered in the radar equation proposed in Section II. These additional parameters are mainly beamshape loss (also called antenna pattern loss), plumbing loss (or connection loss), bandwidth loss, collapsing loss and atmospheric absorption loss. Note that a very exhaustive list of losses is provided by Barton in [34]. In the following we focus on some of these parameters, the reader is invited to consider the reference [34] for more details.

In radar equation (8), the antenna gain G is assumed constant at the maximum of its beam. The calculation of detection probabilities is based on this assumption, considering echoes of constant amplitude. However, in practice, the gain of a scanning antenna in the direction of the target varies from one echo to another, depending on the shape of the antenna beam. **Beamshape losses** (L_b) are used to account for these variations in gain in the radar equation, so that more complex calculations of detection probabilities are not required. When a large number of signal samples are integrated, the appropriate value of beamshape losses is $L_b = 1.6$ dB for an azimuth scanning radar and $L_b = 3.2$ dB for a bidirectional scanning radar [7] [8]. For a non-scanning radar, $L_b = 0$ dB.

Plumbing loss (L_p) includes losses on the transmission lines (or waveguides) that connect the output of the transmitter to the antenna (and inversely the output of the antenna to the receiver), additional losses at the connections or bends in

the lines, or at the rotating joint of the antenna when any. In addition, in the plumbing losses, we can include the mismatch losses related to the standing wave ratio, antenna efficiency and those due to the radome or packaging if any. Transmission line losses are generally small at low frequencies, but, they become significant as frequency increases. Insertion losses of duplexers (or circulators) when used are also included in plumbing losses. For example, Skolnik [7] reported a total plumbing loss $L_p = 3.4$ dB for a radar operating at 3 GHz, including duplexer and joint rotating losses. It should be noted that nowadays, the use of optical rotating joints makes it possible to significantly reduce these losses.

Bandwidth losses or filter mismatch losses (L_m) represent the reduction in SNR at the output of the filter (when a non-optimal receiver bandwidth is used) compared to a matched filter. A bandwidth correction factor is used by Blake [8] to account for these losses in the radar equation. But, Barton [34] has shown that this factor is unsuitable for electronic detection devices. He proposed an adaptation factor taking into account the video bandwidth. However, L_m defined by (50) [34] is more common and seems sufficiently accurate to quantify filter mismatch losses:

$$L_m = \frac{\int_{-\infty}^{+\infty} |A(f)|^2 df \cdot \int_{-\infty}^{+\infty} |H(f)|^2 df}{\int_{-\infty}^{+\infty} |A(f) H(f)|^2 df} \tag{50}$$

where $A(f)$ is the amplitude (in voltage) of the signal spectrum and $H(f)$ the frequency response of the filter. Values of L_m can be found in [34] for an impulse waveform (for different types of filters), but also for linear-FM waveforms (for different weighting functions).

Collapsing losses represent the degradation of the integration gain when N signal-plus-noise samples are integrated with W noise-only samples. Collapsing losses can occur for example, when the range gate (equivalent to the range bin) used for integration is too large so that additional noise samples are included, or when the video bandwidth is insufficient relative to the resolution required to bring out the peak of the useful signal from the noise, or when signals from multiple channels (some of which contain only noise) are combined before detection. In the case of a square law detector, collapsing losses are defined as the ratio of the integration losses for $W+N$ samples to those for N samples as shown in equation (51) [7] [9] [34].

$$L_c(N, W) = \frac{L_i(W+N)}{L_i(N)} \tag{51}$$

Collapsing losses therefore correspond to an increase in SNR_r to maintain the same performance when W noise-only samples are included in the detection (by integration) of N signal-plus-noise samples.

The energy transmitted by a radar operating in long range is partly (in some cases totally) absorbed by atmospheric components. This absorption, which can be neglected at low frequencies, becomes significant, especially in the millimeter band. For example, Abner [35] mentioned that a monostatic radar system operating at 50 GHz with a maximum range of 60 km in free space, will detect the same target with the same detection and false alarm probabilities, at a maximum range of only 19.5 km. **Atmospheric absorption** is mainly due to water vapor and oxygen molecules in the air. It increases with rain, fog, clouds, etc. Atmospheric absorption depends on the frequency, the elevation angle of the considered target, the polarization of the wave, but also on the range. Losses due to atmospheric absorption (L_{at}) must take into account the round-trip path of the wave. The curves for estimating these losses are given in [8]. They show a loss decrease as the elevation angle of the target increases. Rain loss curves are given in [36]. An increase in losses with increasing frequency and intensity of rainfall is observed.

Generally, the attenuation due to more or less strong absorptions of water vapor and oxygen molecules at certain frequencies defines in a certain way the types of applications. Thus, there are the so-called transmission windows around the frequencies 30 GHz, 90 GHz or 220 GHz, which are preferred for long-range applications, and the absorption peaks at 24 GHz, 60 GHz, 118 GHz and 182 GHz where short-range applications are prefered.

VII. Overview

To complete the sizing of radar systems proposed in Section II, it is required to consider fixed threshold or CFAR detection methods discussed in Section IV, integration techniques discussed in Section V, as well as the various losses discussed in Section VI.

On the other hand, for more accuracy, in radar equation (8) the antenna gain G should depend on the direction of observation. To account for this dependence, the antenna propagation factor F is introduced [8]. More generally, this factor includes the antenna gain at the target altitude relative to that on the axis where G is defined, the contribution of surface reflections to the radiated and received fields, and the modification of the fields by diffraction on paths at low altitude [34].

The different losses seen in Section VI can be grouped into two main categories. The first category is those that contribute to the reduction of radar echo energy. These are the so-called system losses $L_S = L_p L_m L_{at}$. The second contains all losses that contribute to the increase in SNR_r. It corresponds to the signal processing losses $L_X = L_b L_i L_c L_d$. The term L_d represents the detection losses. They correspond to CFAR losses (see Figure 11) in the case of CFAR detection. Note that when a fixed threshold detection is used, $L_d = 1$.

Considering integration gain and different losses in system and signal processing, the monostatic radar equation can be written:

$$R_{\max}^4 = \frac{P_{av} T_r \cdot F^4 G^2 \lambda^2 \sigma \cdot G_i(N)}{(4\pi)^3 k_B T \cdot F \cdot SNR_r \cdot L_S \cdot L_X} \tag{52}$$

where SNR_r is the signal-to-noise ratio per sample (for a single radar echo, therefore without integration) according to the target fluctuation model (see Figure 6). The contribution of signal integration is represented here by the integration gain $G_i(N)$ depending on the number of integrated samples and the technique used.

This article has been accepted for publication in a future issue of this journal, but has not been fully edited. Content may change prior to final publication. Citation information: DOI 10.1109/MAES.2022.3177395, IEEE Aerospace and Electronic Systems Magazine

Equation (52) thus completes equation (8), which is the starting point for the sizing of monostatic radar systems. It makes it possible to estimate the maximum detection range by taking into account various significant parameters in the operation of radar systems. This detailed form of the equation not only allows radar system engineers to better understand the influence of each parameter on detection performance, but also allows them to make better choices based on the required specifications in terms of reliability and complexity. Note that this equation is general and should be adapted according to the type of waveform (pulsed, CW or FMCW), the architecture of the radar system and the targeted application.

Finally, we have proposed in this paper a detailed study of radar system sizing. The detection procedure has been described based on the radar equation and its essential parameters. The choice of its parameters has been discussed in relation to the detection methods, the signal integration techniques, but also the performances in terms of system reliability (detection and false alarm probabilities). In addition, the most used target fluctuation models developed by Swerling were taken into account. This study can be completed by a specific analysis according to the desired performances and the specifications in terms of complexity.

Appendix A
Calculation of the SNR in Coherent Integration

N samples are considered in reception and it is assumed that each sample consists of a complex signal $s(t) = A\exp(j\phi)$ and an additive noise of variance ν^2: $y_n(t) = s(t) + b_n(t)$. The signal-to-noise ratio of each sample is then given by:

$$SNR = \frac{A^2}{\nu^2} \tag{53}$$

The signal Y resulting from the sum of the N samples is written as follows:

$$Y(t) = \sum_{n=1}^{N} y_n(t) = Ns(t) + \sum_{n=1}^{N} b_n(t) \tag{54}$$

The total noise power in $Y(t)$ is given by the variance of the sum of the N noise components, i.e. $N\nu^2$. Thus, the signal-to-noise ratio of the signal $Y(t)$, resulting from the coherent integration is written as:

$$SNR = \frac{(NA)^2}{N\nu^2} \tag{55}$$

Expressed as a function of the signal-to-noise ratio per sample (SNR), the SNR_N can then be written as:

$$SNR_N = NSNR \tag{56}$$

Coherent integration of N samples therefore improves the SNR by a factor of N.

Appendix B
Cumulative Probability of Detection using the Wiener Approach for Sw-I and Sw-III Targets

Figure 21 presents a comparison of the ROCs obtained by numerical integration (Integral) and by Wiener's approach (Wiener) for Sw-I and Sw-III targets in the case of cumulative detection. These results are obtained for $P_{FA} = 10^{-6}$ and $N = 10$.

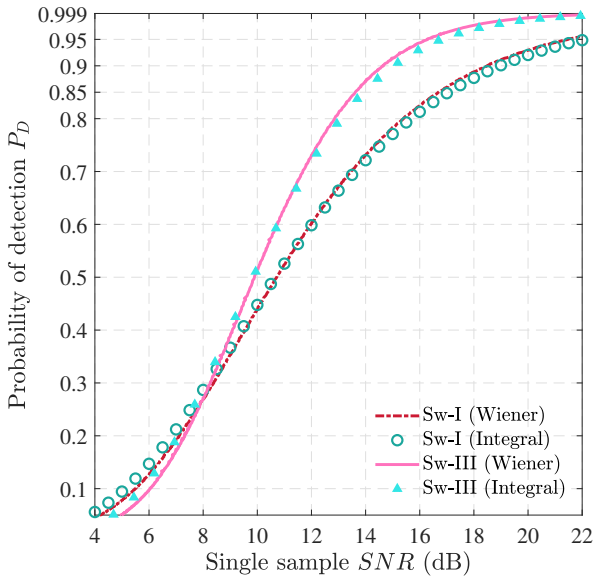

Fig. 21. Comparison of Weiner's approach with numerical integration for Sw-I and Sw-III targets

Appendix C
Integration Losses for Sw-0 Targets

Figure 22 presents a comparison of losses for the integration techniques seen in Section V relative to coherent integration for Sw-0 targets.

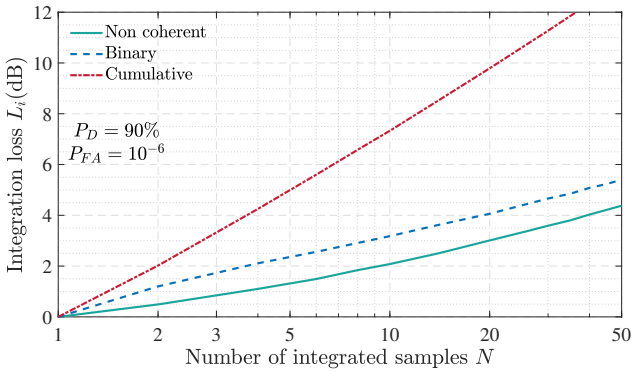

Fig. 22. Comparison of integration loss for different integration techniques in the case of Sw-0 targets

Acknowledgment

The authors would like to thank MORPHEE+ and ESYCOM lab for permitting them to carry out this research.

References

[1] E. F. Knott, J. Shaeffer, and M. Tuley, Eds., *Radar Cross Section*, 2nd ed. Raleigh, NC: SciTech Publishing, Inc., 2004.

[2] V. Borkar, A. Ghosh, R. Singh, and N. Chourasia, "Radar cross-section measurement techniques," *Defence science journal*, vol. 60, pp. 204–212, 03 2010.

[3] J. Marcum, "A statistical theory of target detection by pulsed radar," *IRE Transactions on Information Theory*, vol. 6, no. 2, pp. 59–267, 1960.

[4] P. Swerling, "Probability of detection for fluctuating targets," *IRE Transactions on Information Theory*, vol. 6, no. 2, pp. 269–308, 1960.

[5] D. K. Barton, Ed., *Modern Radar System Analysis*. Norwood, MA: Artech House, Inc., 1988.

[6] J. V. DiFranco and W. L. Rubin, Eds., *Radar Detection*. Artech House, Inc., 1980.

[7] M. I. Skolnik, Ed., *Introduction to Radar Systems*, 2nd ed. McGraw Hill, Inc., 1980.

[8] L. V. Blake, "Recent Advancements in Basic Radar Range Calculation Technique," *IRE Transactions on Military Electronics*, vol. MIL-5, no. 2, pp. 154–164, 1961.

[9] D. K. Barton, "Simple Procedures for Radar Detection Calculations," *IEEE Transactions on Aerospace and Electronic Systems*, vol. AES-5, no. 5, pp. 837–846, 1969.

[10] M. A. Richards, Ed., *Fundamentals of Radar Signal Processing*, 2nd ed. McGraw Hill, Inc., 2005.

[11] P. Swerling, "Radar probability of detection for some additional fluctuating target cases," *IEEE Transactions on Aerospace and Electronic Systems*, vol. 33, no. 2, pp. 698–709, 1997.

[12] E. Lehmann and J. Romano, Eds., *Testing Statistical Hypotheses*, 3rd ed. Springer, 2005.

[13] B. Picinbono and G. Vezzosi, "Extension du critère de Neyman-Pearson en détection d'hypothèses multiples," in *5° Colloque sur le traitement du signal et des images, FRA, 1975*. GRETSI, Groupe d'Etudes du Traitement du Signal et des Images, 1975.

[14] S. O. Rice, "Mathematical analysis of random noise," *The Bell System Technical Journal*, vol. 24, no. 1, pp. 46–156, 1945.

[15] S. Parl, "A new method of calculating the generalized Q function (corresp.)," *IEEE Transactions on Information Theory*, vol. 26, no. 1, pp. 121–124, 1980.

[16] G. R. Curry, Ed., *"Radar System Performance Modeling*, 2nd ed. Artech House Inc., 2005.

[17] G. M. Dillard, "Mean-Level Detection of Nonfluctuating Signals," *IEEE Transactions on Aerospace and Electronic Systems*, vol. AES-10, no. 6, pp. 795–799, 1974.

[18] N. Levanon, Ed., *Radar Principles*. New York: John Wiley & Sons Inc, 1988.

[19] H. Meikle, Ed., *"Modern Radar Systems*, 2nd ed. Artech House, 2008.

[20] H. Rohling, "Radar CFAR Thresholding in Clutter and Multiple Target Situations," *IEEE Transactions on Aerospace and Electronic Systems*, vol. AES-19, no. 4, pp. 608–621, 1983.

[21] M. Weiss, "Analysis of Some Modified Cell-Averaging CFAR Processors in Multiple-Target Situations," *IEEE Transactions on Aerospace and Electronic Systems*, vol. AES-18, no. 1, pp. 102–114, 1982.

[22] J. T. Rickard and G. M. Dillard, "Adaptive Detection Algorithms for Multiple-Target Situations," *IEEE Transactions on Aerospace and Electronic Systems*, vol. AES-13, no. 4, pp. 338–343, 1977.

[23] R. Nitzberg, "Analysis of the Arithmetic Mean CFAR Normalizer for Fluctuating Targets," *IEEE Transactions on Aerospace and Electronic Systems*, vol. AES-14, no. 1, pp. 44–47, 1978.

[24] V. G. Hansen and J. H. Sawyers, "Detectability Loss Due to "Greatest Of" Selection in a Cell-Averaging CFAR," *IEEE Transactions on Aerospace and Electronic Systems*, vol. AES-16, no. 1, pp. 115–118, 1980.

[25] C. H. Lim and H. S. Lee, "Performance of order-statistics CFAR detector with noncoherent integration in homogeneous situations," *IEE Proceedings F - Radar and Signal Processing*, vol. 140, no. 5, pp. 291–296, 1993.

[26] M. Shor and N. Levanon, "Performances of order statistics CFAR," *IEEE Transactions on Aerospace and Electronic Systems*, vol. 27, no. 2, pp. 214–224, 1991.

[27] S. Blake, "OS-CFAR theory for multiple targets and nonuniform clutter," *IEEE Transactions on Aerospace and Electronic Systems*, vol. 24, no. 6, pp. 785–790, 1988.

[28] J. Pachares, "A table of bias levels useful in radar detection problems," *IRE Transactions on Information Theory*, vol. 4, no. 1, pp. 38–45, 1958.

[29] R. B. Mahafza, Ed., *Radar system & analysis and design using Matlab*, 2nd ed. CRC Press 2000, 2000.

[30] P. Surendran, J.-H. Lee, and S. J. Ko, *Performance of Non-coherent Detectors for Ultra Wide Band Short Range Radar in Automobile Applications*. Springer-Verlag Berlin Heidelberg, 2012, vol. 377, pp. 185–195 in Software Engineering Research, Management and Applications 2011, ISBN: 978-3-642-23201-5.

[31] M. A. Weiner, "Binary integration of fluctuating targets," *IEEE Transactions on Aerospace and Electronic Systems*, vol. 27, no. 1, pp. 11–17, 1991.

[32] D. A. Shnidman, "Binary integration for swerling target fluctuations," *IEEE Transactions on Aerospace and Electronic Systems*, vol. 34, no. 3, pp. 1043–1053, 1998.

[33] N. Johnson, "Cumulative detection probability for swerling III and IV targets," *Proceedings of the IEEE*, vol. 54, no. 11, pp. 1583–1584, 1966.

[34] D. K. Barton, Ed., *Radar Equations for Modern Radar*. Artech House, Inc., 2013.

[35] D. A. Ephrath, "Atmospheric loss considerations in radar range equations," in *Digest on Antennas and Propagation Society International Symposium*, 1989, pp. 831–833 vol.2.

[36] G. R. Curry, Ed., *Radar Essentials, A Concise Handbook for Radar Design and Performance Analysis*. SciTech Publishing, Inc., 2012.

Pape Sanoussy Diao received the M. Sc. in Electronics Telecommunications and Geomatics, speciality High Frequency Communication Systems from Université Paris-Est Marne-la-Vallée, France, in 2015 and the Ph.D. degree in Electronics, Optronic and Systems from University Paris-Est, France, in 2019. He joined the company MORPHEE+ in 2019 as a researcher. He is particularly interested in radar detection and associated processing, RF systems, architectures and mm-wave technologies.

Thierry Alves received the M. Sc. degree in microelectronics from University Bordeaux I, France, in 2007 and the Ph.D. degree in Electronics, Optronic and Systems from University Paris-Est, France, in 2011. He is an ENSEIRB Engineer in electronics and radiocommunications. Dr Alves was researcher in ONERA. He is currently associate professor in ESIEE Paris, Université Gustave Eiffel. His research include small antenna design in lossy environments, lightning, earth-ionosphere waveguide, channel characterization, RF systems & architectures.

Benoit Poussot is Electronic Engineer of the ESPCI-CNAM (2004), he obtained his Ph.D. in Electronics from Université Paris-Est Marne-la-Vallée, in 2007. He is currently associate professor at Université Gustave Eiffel. Dr Poussot has authored or co-authored more than 40 publications, communications, technical reports, patents and book chapters. His research include wave propagation, channel modelling, reconfigurable antenna design, systems & architectures for 60 GHz applications and detection & localisation techniques.

Sylvain Azarian has an M. Sc. degree in fundamental computer science from University Paris VI. He was researcher in ONERA in the Electromagnetism & Radar Department and Director of the Sondra research lab in CentraleSupelec, the Electrical Engineering school of the Paris-Saclay University. He joined the company in 2019 as part of the technology transfer between ONERA and MORPHEE+ where he is now Chief Technical Officer. Since 2021, he is also the president of the International Amateur Radio Union (Region 1).